Journal of Molecular Liquids 368 (2022) 120773

Contents lists available at ScienceDirect

Journal of Molecular Liquids

journal homepage: www.elsevier.com/locate/molliq

Molecular dynamics investigations into the hydrogen permeation mechanism of polyethylene pipeline material

Dukui Zheng [a], Jingfa Li [b,*], Bing Liu [a,*], Bo Yu [b], Yafan Yang [c], Dongxu Han [b], Jianli Li [b], Zhiqiang Huang [a]

[a] College of Petroleum Engineering, Yangtze University, Wuhan 430100, China
[b] School of Mechanical Engineering and Hydrogen Energy Research Center, Beijing Institute of Petrochemical Technology, Beijing 102617, China
[c] State Key Laboratory for Geomechanics and Deep Underground Engineering, China University of Mining and Technology, Xuzhou 221116, China

ARTICLE INFO

Article history:
Received 16 August 2022
Revised 29 October 2022
Accepted 6 November 2022
Available online 17 November 2022

Keywords:
Hydrogen
Polyethylene
Solubility
Diffusion
Permeability
Molecular dynamics simulation

ABSTRACT

To avoid hydrogen embrittlement and other hydrogen damage caused during hydrogen transportation using metal pipelines, it is feasible to transport hydrogen through nonmetallic polyethylene (PE) pipelines. However, gas permeation and leakage are more obvious for hydrogen delivery using PE pipelines than those using metal pipelines. To reveal the permeation and diffusion mechanisms of hydrogen in PE pipelines, the Grand Canonical Monte Carlo simulation and molecular dynamics are conducted. The solubility and diffusion characteristics of hydrogen in amorphous PE are investigated at temperatures of 270–310 K and pressures of 0.1–0.7 MPa. The influences of temperature and pressure on hydrogen permeation are also analyzed. The results show that the solubility, diffusion, and permeability coefficients of hydrogen in amorphous PE increase with increasing temperature, and their relationships with temperature are consistent with the Arrhenius law. Pressure has a negligible effect on the permeability coefficient of hydrogen in amorphous PE, whereas temperature appreciably affects the permeability coefficient. The diffusion of hydrogen in PE conforms to the "hopping" mechanism. The hydrogen molecule vibrates in the free volume pore for a long time and then quickly hops to the adjacent pores to complete diffusion. The hydrogen molecule continues to vibrate and hop, eventually moving further away from its initial position and permeating through PE materials.

1. Introduction

With the proposal of carbon peaking and carbon neutrality goals in China, the development of clean energy to reduce carbon emissions has become a trend for future development in the energy industry. Hydrogen energy has been widely studied in recent years as a clean energy source with great development potential. It has significant advantages over traditional fossil fuels, such as being a clean, non-carbon, efficient, renewable energy source and having various application modes. Therefore, the development of strategies for H_2 energy production is an important measure for reducing global carbon emissions. The delivery of H_2 is an important factor in the H_2 energy industry. Among the commonly used H_2 delivery methods, it is economical and efficient to transport H_2 through pipelines [1,2]. However, hydrogen embrittlement and other hydrogen-induced damages will occur when using metal pipelines to transport H_2, which can lead to serious safety problems [3,4]. While polyethylene (PE) pipelines can effectively overcome the problems associated with the use of metal pipelines. In addition, PE pipelines possess the advantages of lightweightness, easy installation, and low cost [5]. However, compared to metal pipelines, PE pipelines are more prone to gas permeation. As H_2 is a flammable and explosive gas, long-term gas permeation not only causes energy loss and waste but also increases the risk of combustion and explosion after gas permeation and leakage. Therefore, it is of great significance to study the hydrogen permeation mechanism in PE pipelines to ensure the safe transportation of H_2 through pipelines.

As a type of thermoplastic materials, PE has the characteristics of high corrosion resistance, chemical stability, and toughness; hence, it has been used in a wide range of applications, such as in food bags and pipelines. To apply PE for gas transportation, understanding its gas permeability is of significance. Thus, some scholars have studied the permeability characteristics of gases in amorphous PE using molecular dynamics (MD). For example, Sun et al. [6] focused on the diffusion of five flavor organic gas molecules in amorphous PE, including d-limonene, myrcene, ethyl hexanoate, 2-nonanone, and linalool, and the influence of their

* Corresponding authors.
E-mail addresses: lijingfa@bipt.edu.cn (J. Li), lb951782259@163.com, lb951782259@163.com (B. Liu).

https://doi.org/10.1016/j.molliq.2022.120773
0167-7322/

presence on the diffusion of O_2 in amorphous PE was revealed. The simulated results were found to be close to the experimental results. Börjesson et al. [7] used the Monte Carlo (MC) simulation and MD to study the solubility and diffusion of O_2 in amorphous PE at a pressure of 0.1 MPa and temperatures of 270–308 K. The solubility coefficient of O_2 in amorphous PE decreased with increasing temperature, while the diffusion coefficient showed the opposite trend. Dutta et al. [8] studied and compared the solubility and diffusivity of CO_2, CH_4, and N_2 in amorphous PE at 300––600 K, using the Grand Canonical Monte Carlo (GCMC) simulation and MD. Yang et al. [9] simulated the dissolution and diffusion behaviors of CH_4 and CO_2 in amorphous PE over wide temperature (350–600 K) and pressure (0.1–50 MPa) ranges. The simulated values for dissolution were qualitatively consistent with the experimental values, and the simulated values for diffusion matched the experimental results well.

H_2 is one of the most ideal new energy sources for the future. Therefore, some scholars have studied the dissolution, diffusion, and permeation behaviors of H_2 in various materials through MD. Hassanzadeh et al. [10] explored the dissolution and diffusion behaviors of H_2 in Mobil-FIve (MFI) zeolites based on the GCMC and MD simulations. The solubility coefficient of H_2 decreased with an increase in temperature, whereas the diffusion coefficient showed the opposite trend. However, the relationships of the aforementioned two coefficients with the increase in pressure showed irregularity. Tan et al. [11] analyzed and compared the solubility, diffusivity, and permeability of H_2, N_2, O_2, CO_2, and CH_4 in hydrogenated nitrile butadiene rubber (HNBR) and ethylene-ethene-diene rubber (EPDM). The simulation results demonstrated that H_2 has the smallest solubility coefficient, largest diffusion coefficient, and largest permeability coefficient among the five types of gases in HNBR and EPDM. Brunetti et al. [12] investigated the solubility and diffusivity of H_2, CO_2, N_2, CH_4, and CO and their binary mixtures in thermally rearranged poly (benzoxazole-*co*-imide) through experiments and MD, and revealed the interactions of the mixed gases during dissolution and diffusion. Yi et al. [13] compared the diffusion performances of H_2, D_2, and T_2 in polystyrene with different degrees of polymerization. Azizi et al. [14] simulated the solubility, diffusion, and permeability coefficients of H_2, CO_2, CO, and H_2O in polyurethane; the results were in good agreement with the experimental results. Similarly, Bian et al. [15] investigated the dissolution and diffusion characteristics of H_2, He, N_2, O_2, Cl_2, CO_2, H_2S, SO_2, and H_2O in a poly-*para*-xylylene polymer.

Currently, many simulation studies have been conducted on the dissolution, diffusion, and permeation of other gases in PE or H_2 in other materials. However, studies on the permeability of H_2 in PE are mostly based on membrane permeability experiments [16–18] and full-scale permeability experiments [19–21]. Numerical simulation studies have rarely been reported in the literature. In addition, there are some shortcomings in studying the H_2 permeability in PE using experimental methods, such as a long experimental period, high cost, and the risk of gas leakage and explosion. However, the numerical simulation approach can overcome these shortcomings. MD simulations are currently the main research method for studying gas permeability in polymer materials [22–25]. It is convenient to observe the gas permeation and morphological changes of polymers at the nanoscale using MD simulations [26]. To explore the H_2 permeation and diffusion mechanisms in PE pipelines, in this study, the combination of MD and the GCMC simulation is adopted to study the diffusion, dissolution, and permeation characteristics of H_2 molecules in amorphous PE under common transportation conditions (temperatures of 270–310 K and pressures of 0.1–0.7 MPa) of urban gas PE pipelines. The simulation results can be used to guide the determination of transportation conditions and the selection of PE materials to reduce the permeability of H_2 in PE pipelines, so as to ensure the safe transportation of H_2 in PE pipelines.

The remainder of this paper is organized as follows. In Section 2, the modeling process and optimization steps for the H_2 molecule and amorphous PE cell are described in detail. Section 3 introduces the force field used in MD. In Section 4, the simulation method and calculation process for the solubility, diffusion, and permeability coefficients of H_2 in amorphous PE are presented. In Section 5, the simulation results are discussed and analyzed, including the glass transition temperature of amorphous PE cells; the effects of temperature and pressure on the solubility, diffusion, and permeability coefficients of H_2 in amorphous PE; and the diffusion mechanism. Finally, the concluding remarks of this study are summarized in Section 6.

2. Molecular dynamics model

PE single chain with 500 polymerization degrees (i.e., $C_{1000}H_{2002}$) and H_2 molecule are constructed using the all-atom model with high precision. Then, the structures of the PE single chain and H_2 molecule are optimized with 500 steps. The ten three-dimensional periodic amorphous PE cells, each containing five PE chains, are constructed on the basis of Theodorou and Suter's modified rotational isomeric state method [27,28]. The amorphous PE cell with the lowest energy is selected from the ten amorphous PE cells, and then is optimized with 10,000 steps to eliminate the unreasonable structure, in which the target energy and force are 1×10^{-4} kcal/mol and 5×10^{-3} kcal/mol/Å, respectively.

Geometric optimization is only a rough optimization method; therefore, a series of dynamic operations are needed to relax the amorphous PE cell for equilibrium, as shown below. (1) The NVT ensemble is used for 500 ps relaxation at 300 K. (2) An annealing operation with six annealing cycles is carried out. In each cycle, the temperature is increased from 300 to 600 K with a temperature step of 60 K and then decreased to 300 K with the same temperature step. A total of 3000 ps of NPT relaxation (0.1 MPa) is carried out during the entire annealing process, in which 50 ps of NPT relaxation is carried out at each temperature in the cycle. (3) The NPT ensemble is used to relax the amorphous PE cell for 500 ps at 300 K and 1 GPa. (4) The NPT ensemble is used to balance for 1000 ps at 298 K and 0.1 MPa. In the MD simulation process, the temperature and pressure are controlled using a Nose thermostat and a Berendsen barostat. The velocity Verlet algorithm is used for dynamic integration. The time step is 1 fs, and the initial velocity is generated using the Maxwell-Boltzmann distribution. The van der Waals interaction force and the electrostatic interaction force are calculated by the "Group Based" [13,29] with a cutoff radius of 15.5 Å and a spline width of 1 Å. According to above settings and operations, the final size of the amorphous PE cell at normal temperature and pressure is $52.65 \times 52.65 \times 52.65$ Å, as shown in Fig. 1. The final density of the amorphous PE cell is 0.795 g/cm^3, which is 7.02 % lower than the actual density of 0.855 g/cm^3 [30] and close to the value of 0.805 g/cm^3 simulated by Dutta [8]. This error is within the allowable range, indicating that the established amorphous PE cell model is reasonable.

3. Molecular dynamics force field

The selection of the force field has an important influence on the accuracy of the MD results. In this study, a polymer consistent force field (PCFF) suitable for polymers is adopted in the simulation [31,32]. In the PCFF, the total energy is divided into bond energy and non-bond energy:

$$E_{\text{total}} = E_{\text{bond}} + E_{\text{non-bond}} \quad (1)$$

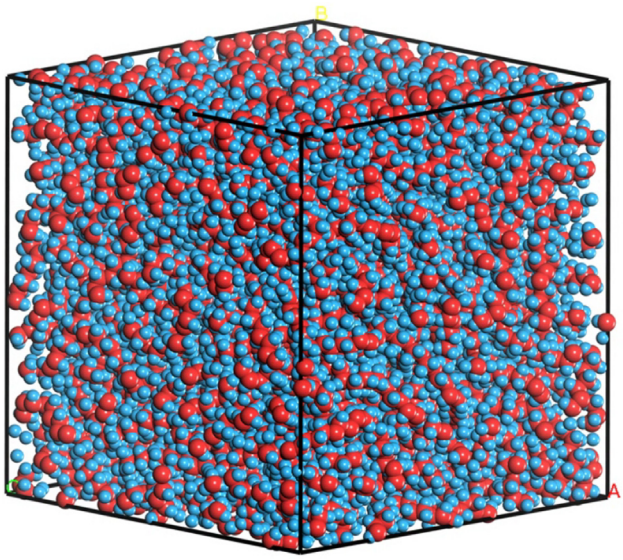

Fig. 1. Amorphous PE cell (carbon atoms are blue; hydrogen atoms are red).

where E_{total} is the total energy, kcal/mol; E_{bond} is the bond energy, kcal/mol. For H_2, E_{bond} contains the bond stretching energy, as shown in Eq. (2a). For PE, E_{bond} contains the bond stretching energy, valence angle bending energy, dihedral angle torsion energy, inversion energy, and cross-term energy, as shown in Eq. (2b); $E_{non\text{-}bond}$ is the non-bond energy, including the electrostatic energy and van der Waals energy, as shown in Eq. (3).

$$E_{bond} = E_b \tag{2a}$$

$$E_{bond} = E_b + E_\theta + E_\varphi + E_\chi + E_{cross} \tag{2b}$$

$$E_{non-bond} = E_c + E_v \tag{3}$$

In these equations, E_b is the bond stretching energy, kcal/mol; E_θ is the valence angle bending energy, kcal/mol; E_φ is the dihedral angle torsion energy, kcal/mol; E_χ is the inversion energy, kcal/mol; E_{cross} is the cross-term energy, kcal/mol; E_c is the electrostatic energy, kcal/mol; E_v is the van der Waals energy, kcal/mol. In this study, the Lennard-Jones (L-J) 9-6 model is used to calculate the van der Waals energy between the two atoms:

$$E_{ij} = \varepsilon_{ij}\left[2\left(\frac{\sigma_{ij}}{r_{ij}}\right)^9 - 3\left(\frac{\sigma_{ij}}{r_{ij}}\right)^6\right] \tag{4}$$

where E_{ij} is the van der Waals energy between atom i and atom j, kcal/mol; ε_{ij} is the equilibrium well depth between atom i and atom j, kcal/mol; σ_{ij} is the equilibrium distance between atom i and atom j, Å; r_{ij} is the distance between atom i and atom j, Å. The values of ε_{ij} and σ_{ij} are calculated by the "Sixth power" van der Waals combination rule, as shown in Eqs. (5) and (6), respectively:

$$\varepsilon_{ij} = \sqrt{\varepsilon_i \varepsilon_j}\,\frac{2\sigma_i^3\sigma_j^3}{\sigma_i^6 + \sigma_j^6} \tag{5}$$

$$\sigma_{ij} = \sqrt[6]{\left(\frac{\sigma_i^6 + \sigma_j^6}{2}\right)} \tag{6}$$

where ε_i and ε_j are the equilibrium well depth of atom i and atom j, respectively, kcal/mol; σ_i and σ_j are the equilibrium distance of atom i and atom j, respectively, Å. In the PCFF, the ε_C, ε_H, σ_C, and σ_H values of PE are 0.054 kcal/mol, 0.02 kcal/mol, 4.01 Å and 2.995 Å, respectively. The values of ε_H and σ_H for H_2 are 0.02 kcal/mol and 2.995 Å, respectively. According to the above-mentioned parameters, the van der Waals energy of any two atoms in the PE cell with a distance smaller than the cutoff radius (15.5 Å) can be calculated using Eqs. (4)–(6).

4. Molecular dynamics simulation process

4.1. Simulation of dissolution/sorption process

Based on the GCMC simulation, the adsorption isotherms and solubility coefficients of H_2 in amorphous PE at different temperatures are studied. The ensemble used for the GCMC simulation is the μVT ensemble. In the GCMC simulation process, the Metropolis method is adopted to insert, delete, translate, and rotate H_2 molecules [15], to determine the dissolved concentration of gas molecules when the chemical potential of gas molecules in the gas phase is equal to that of gas molecules in the polymer phase. At the same temperature, the adsorption isotherm is obtained according to the dissolved concentrations corresponding to different fugacities. The adsorption isotherm of H_2 in amorphous PE can be fitted using the Henry model, as shown in Eq. (7). When the fugacity tends to 0, the limit slope of the adsorption isotherm represents the solubility coefficient, as shown in Eq. (8).

$$C = K_H \cdot f \tag{7}$$

$$S = \lim_{f\to 0}\frac{C}{f} = K_H \tag{8}$$

Here C is the dissolved concentration of the gas molecules in the polymer, $cm^3(STP)/cm^3$; K_H is the Henry constant; f is the fugacity, MPa; S is the solubility coefficient, which represents the thermodynamic characteristics between gas molecules and polymers, $cm^3(STP)/(cm^3 \cdot MPa)$.

Using the Metropolis method, the H_2 molecules are inserted, deleted, and translated, with the probabilities of 40 %, 40 %, and 20 %, respectively. After the gas molecules are inserted, deleted, and translated, the acceptance probability of the new configuration can be calculated using Eqs. (9)–(11) [14,33].

$$P_{acc} = \min\left[1, \frac{f_i V}{(N_i+1)K_B T}\cdot\exp\left(-\frac{\Delta E}{K_B T}\right)\right] \tag{9}$$

$$P_{acc} = \min\left[1, \frac{N_i K_B T}{f_i V}\cdot\exp\left(-\frac{\Delta E}{K_B T}\right)\right] \tag{10}$$

$$P_{acc} = \min\left[1, \exp\left(-\frac{\Delta E}{K_B T}\right)\right] \tag{11}$$

Here P_{acc} is the acceptance probability of the new configuration; f_i is the fugacity of gas component i; V is the cell volume; N_i is the number of current molecules in gas component i; K_B is the Boltzmann constant; T is the temperature; ΔE is the energy change from the old to new configuration.

In this study, 2×10^7 steps are performed in the simulation, where the first 1×10^7 steps are the equilibration steps and the last 1×10^7 steps are the production steps. The fugacity range is 100–1000 kPa, and the fugacity step is 100 kPa. Three independent PE cells are simulated at each temperature, and each PE cell is simulated at least five times to reduce the errors.

4.2. Simulation of diffusion process

In this study, the diffusion of H_2 in amorphous PE is investigated through MD simulations. The mean square displacement (MSD) versus time (t) figure of H_2 in amorphous PE is obtained by long-term dynamic simulation. The diffusion coefficient can be calcu-

lated using the Einstein equation for the normal diffusion part in the MSD-t figure.

$$D = \frac{1}{6N_a} \lim_{t\to\infty} \frac{d}{dt} \sum_{i=1}^{N_a} \langle |r_i(t) - r_i(0)|^2 \rangle \quad (12)$$

$$D = \frac{a}{6} \quad (13)$$

Here D is the diffusion coefficient, representing the dynamic characteristics between gas molecules and polymers, cm^2/s; N_a is the number of gas molecules; $r_i(t)$ is the coordinate of gas molecule i at time t; and $r_i(0)$ is the coordinate at initial time of the gas molecule i; $\langle ... \rangle$ is the ensemble average of MSD; a is the slope of the normal diffusion part of the MSD-t figure. The value of $\left\langle |r_i(t) - r_i(0)|^2 \right\rangle$ is proportional to t^n.

By linear fitting different segments of the log(MSD) – log(t) figure, different slopes n represent different diffusion processes. When n is less than 1, it denotes abnormal diffusion, which implies that the gas molecule vibrates in the pore. When n is equal to 1, normal diffusion occurs, which indicates that the gas molecule diffuses to the adjacent pore. When n is greater than 1, ballistic diffusion occurs, indicating that the gas molecule does not hit the polymer during movement [34]. The solution process of the diffusion coefficient is presented as follows: (1) find the part with a slope of 1 in the log(MSD) – log(t) figure; (2) obtain slope a by linear fitting of this part in the MSD-t figure; (3) calculate the diffusion coefficient through Eq. (13).

In the simulation of gas diffusion, some scholars inserted an artificially determined number of gas molecules into a polymer cell to study the gas diffusion coefficient [35,36]. However, inserting different numbers of gas molecules affects the cell volume, which further affects the gas diffusion coefficient. To obtain accurate diffusion coefficients of H_2, in this study, an amorphous PE cell adsorbed with H_2 is used as the initial configuration for the study of the diffusion coefficient. The number of H_2 molecules in the amorphous PE cell is obtained by considering the dissolution of H_2 in amorphous PE; therefore, the results will be more reasonable. Three independent PE cell under each working condition performed at least five NVT operations with 5 ns, and the final diffusion coefficient is the average result calculated from the MSD-t curves to reduce the simulation errors. The time step is 1 fs, and the frames are outputted every 500 steps. The other conditions are the same as those described in Section 2.

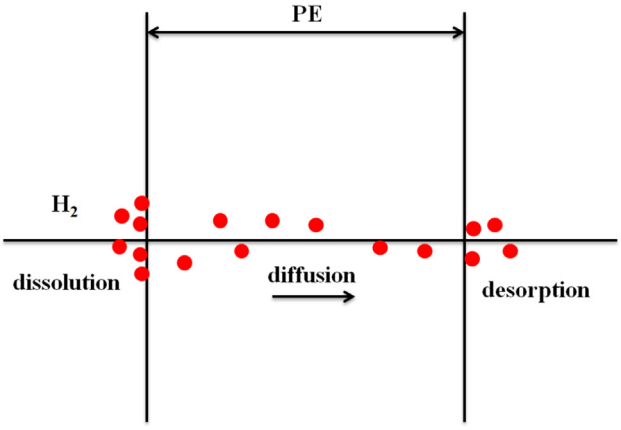

Fig. 2. Process of H_2 permeation in PE.

4.3. Simulation of permeation process

The permeation process of H_2 in PE can be described by the "dissolution-diffusion" theory, as shown in Fig. 2. The H_2 molecules dissolve into PE from the surface, and diffuse in PE from one side to the other. Finally, H_2 molecules are desorbed, allowing the escape of PE [37]. Therefore, the H_2 permeation process in PE can be divided into dissolution and diffusion processes. The relationship among the solubility, diffusion, and permeability coefficients can be described by Eq. (14).

$$P = SD \quad (14)$$

Here P is the permeability coefficient, cm^3(STP)·cm/(cm^2·s·MPa); S is the solubility coefficient, cm^3(STP)/(cm^3·MPa); D is the diffusion coefficient, cm^2/s.

5. Analysis of simulation results

5.1. Glass transition temperature

According to the temperature difference, PE can be considered to have the following three states: the glass state, rubbery state, and viscous state; the transition temperature from the glass state to the rubbery state is T_g. When PE is in the glass state, it exhibits hardness and brittleness. When PE is in the rubbery state, it has a degree of flexibility and can be used as a transportation pipeline. When the temperature reaches T_g in the process of PE changing from the glass state to the rubbery state, the specific volume, v, of PE significantly changes. In this study, MD is conducted to explore the T_g of amorphous PE. The dynamic operation of "NVT + NPT" is carried out 11 times on the amorphous PE cell, reducing the temperature from 355 K to 55 K with a temperature step of 30 K. It is clear that the first six and last five specific volumes have a good linear relationship with temperature; the volumes are fitted linearly, and the intersection point of these two fitting lines is denoted as T_g, as shown in Fig. 3. At each temperature, the NVT and NPT ensembles are operated for 500 and 1000 ps, respectively. The other operating conditions are described in Section 2.

Fig. 3 shows that T_g obtained by MD is 225.64 K, which is within the range of experimental results (200–250 K) [38]. The fitting degree of the data before and after T_g is good, which again shows that the established amorphous PE cell is reasonable.

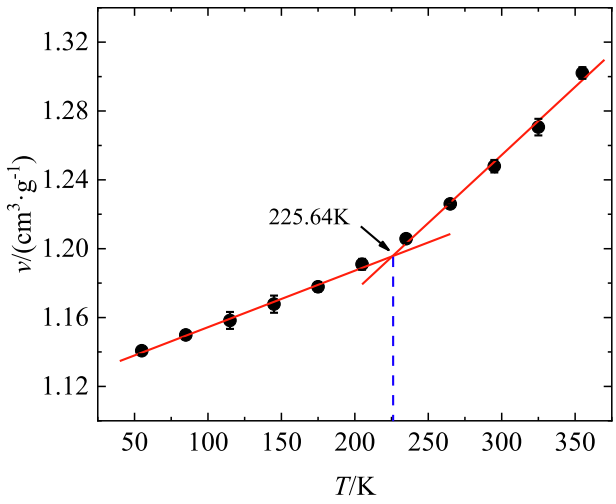

Fig. 3. Glass transition temperature of the amorphous PE cell.

5.2. Influences of temperature on the solubility coefficient

The adsorption isotherms of H_2 in amorphous PE at 270, 280, 290, 300, and 310 K are calculated based on the GCMC simulation, as shown in Fig. 4. The solubility coefficients of H_2 in amorphous PE at different temperatures are calculated using Eq. (8), as shown in Fig. 5. Figs. 4 and 5 show that the slope of the adsorption isotherm increases with increasing temperature, that is, the solubility coefficient of H_2 in amorphous PE increases with an increase in temperature. Generally, the solubility coefficient of a gas increases with a decrease in temperature. However, gases with a low critical temperature, such as H_2 and N_2, show an opposing trend called "reverse solubility" [39,40]. This abnormal phenomenon occurs because it is difficult to dissolve gases with low critical temperatures into PE at low temperatures. However, the free volume in PE increases with an increase in temperature, which increases the chance for gases with low critical temperatures to dissolve into PE.

It should be noted that the solubility coefficients of H_2 in amorphous PE with zero crystallinity are studied in this study; however, a certain amount of crystallinity is present in real PE. The degree of crystallinity affects the solubility coefficient of H_2 in PE because H_2 only dissolves in the amorphous region of PE but not in the crystalline region. The relationship between the solubility coefficient of H_2 in amorphous PE and real PE is shown below in Eq. (15) [41].

$$S_a = \frac{S_s}{\theta_a} \tag{15}$$

Here S_a is the solubility coefficient of H_2 in amorphous PE materials, $cm^3(STP)/(cm^3{\cdot}MPa)$; S_s is the solubility coefficient of H_2 in semi-crystalline PE materials, $cm^3(STP)/(cm^3{\cdot}MPa)$; θ_a is the volume fraction of the amorphous region, %.

To validate the MD results, the solubility coefficients of H_2 obtained in this study are compared with those of H_2 in semi-crystalline PE experimentally studied by Ash [42], Chen [43], Naito [44], Deas Jr [45], and Kubo [46]. The results are transformed to the solubility coefficients of H_2 in amorphous PE according to Eq. (15), as shown in Fig. 6. Fig. 6 shows that the solubility coefficients obtained by MD in this study are within the range of those obtained by experiments, which illustrates that the simulation results are reasonable.

The relationship between the solubility coefficients and temperatures of H_2 in amorphous PE can be expressed by the Arrhenius law, as shown in Eq. (16). The fitting results are shown in Fig. 7; the

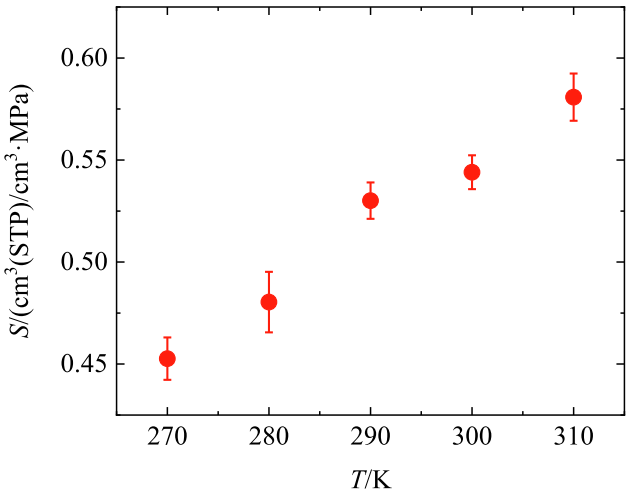

Fig. 5. Solubility coefficients of H_2 in amorphous PE at different temperatures.

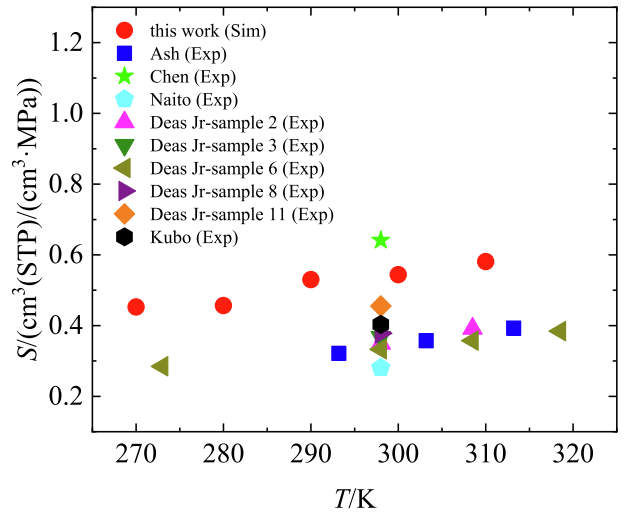

Fig. 6. Comparison of solubility coefficients obtained by MD simulations and experiments.

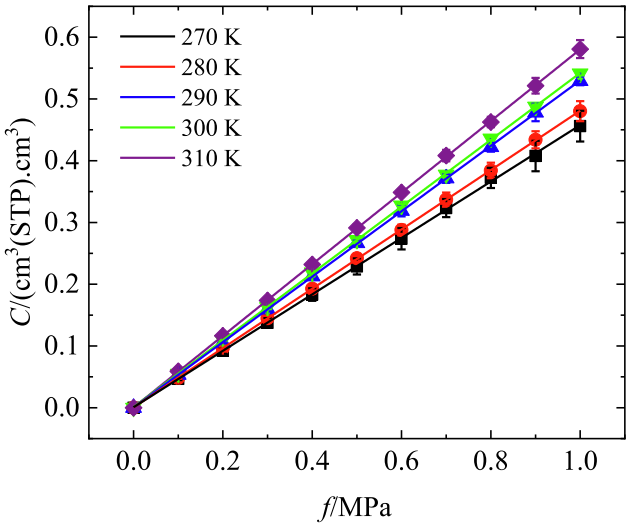

Fig. 4. Adsorption isotherms of H_2 in amorphous PE at different temperatures.

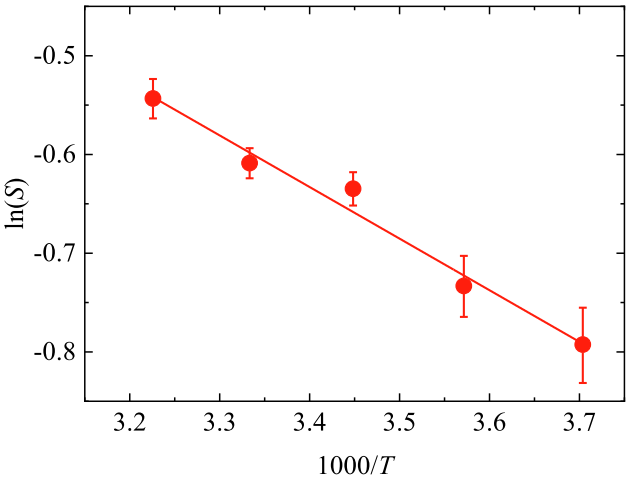

Fig. 7. Relationship between solubility coefficients and temperatures fitted by the Arrhenius law.

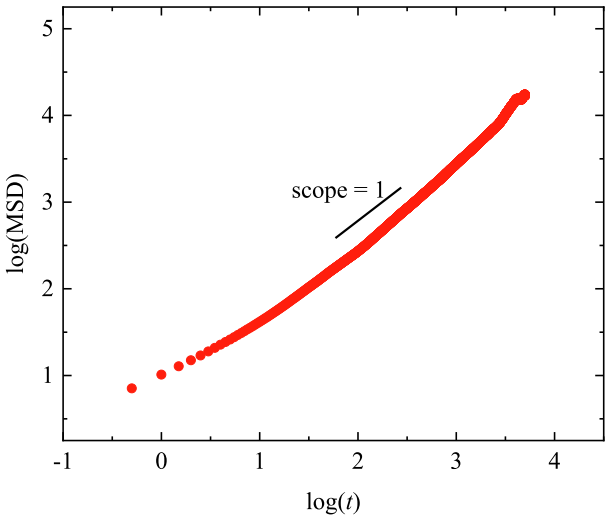

Fig. 8. Log(MSD) – log(t).

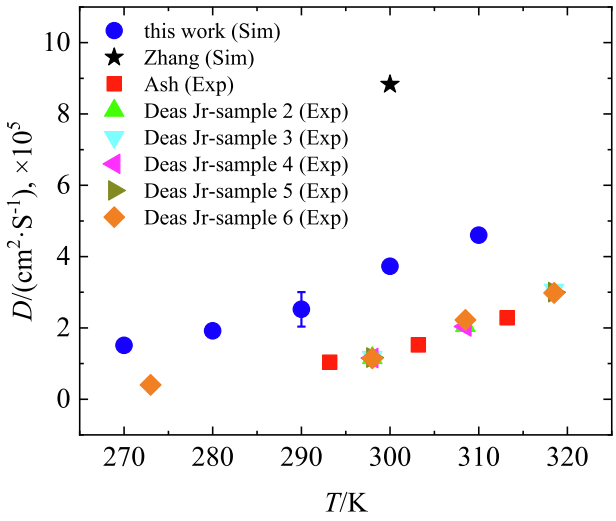

Fig. 10. Comparison of diffusion coefficients obtained by MD simulations and experiments at 0.1 MPa.

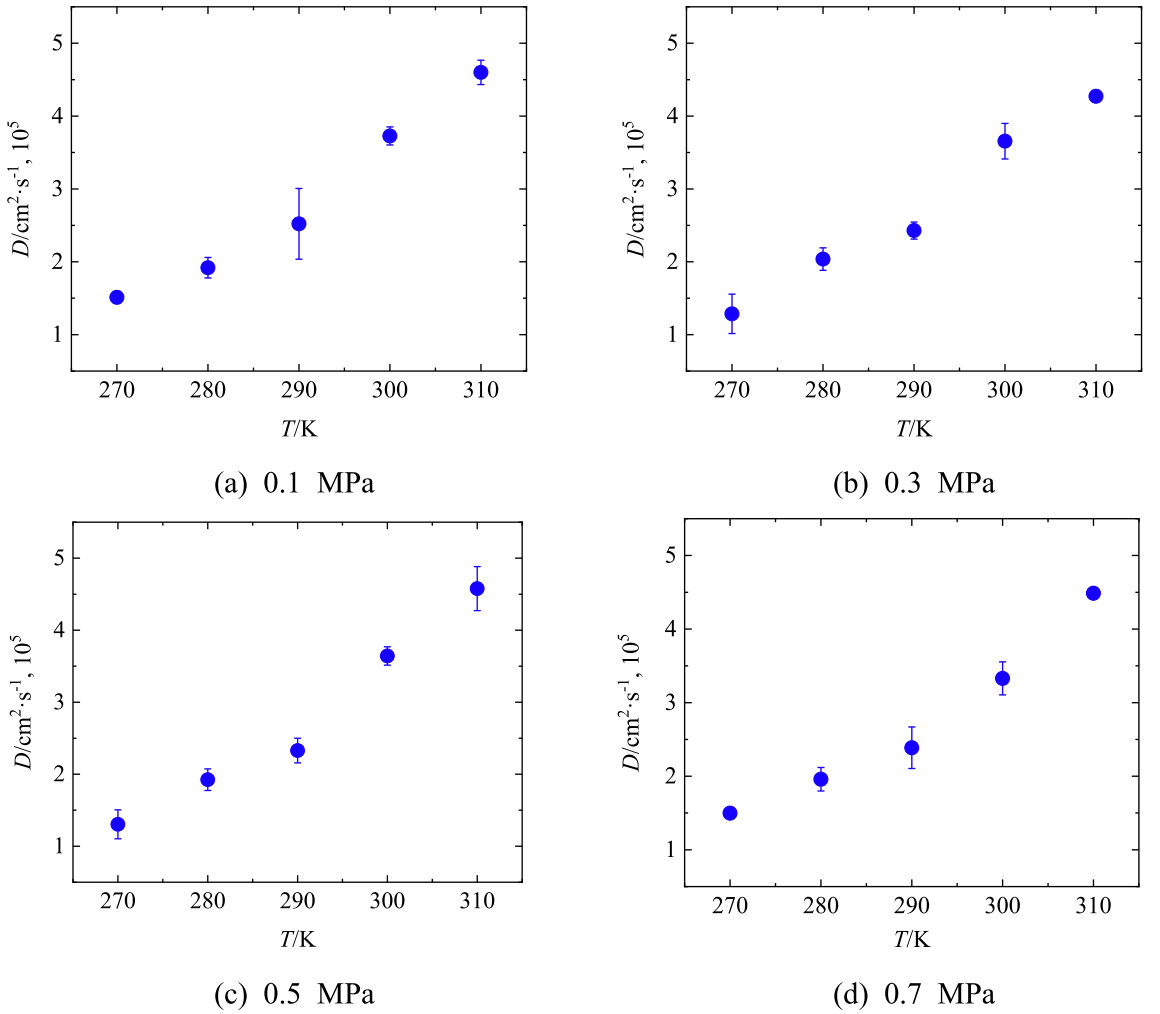

Fig. 9. Diffusion coefficients of H_2 at the temperatures of 270–310 K.

logarithm of the solubility coefficients is linear with the reciprocal of temperature. Thus, when PE is in the rubbery state, the solubility coefficients corresponding to other temperatures can be inferred from the Arrhenius law.

$$S = S_0 \times \exp(-\frac{\Delta H_s}{RT}) \quad (16)$$

Here S is the solubility coefficient, $cm^3(STP)/(cm^3 \cdot MPa)$; S_0 is the pre-exponential factor corresponding to the solubility coefficient,

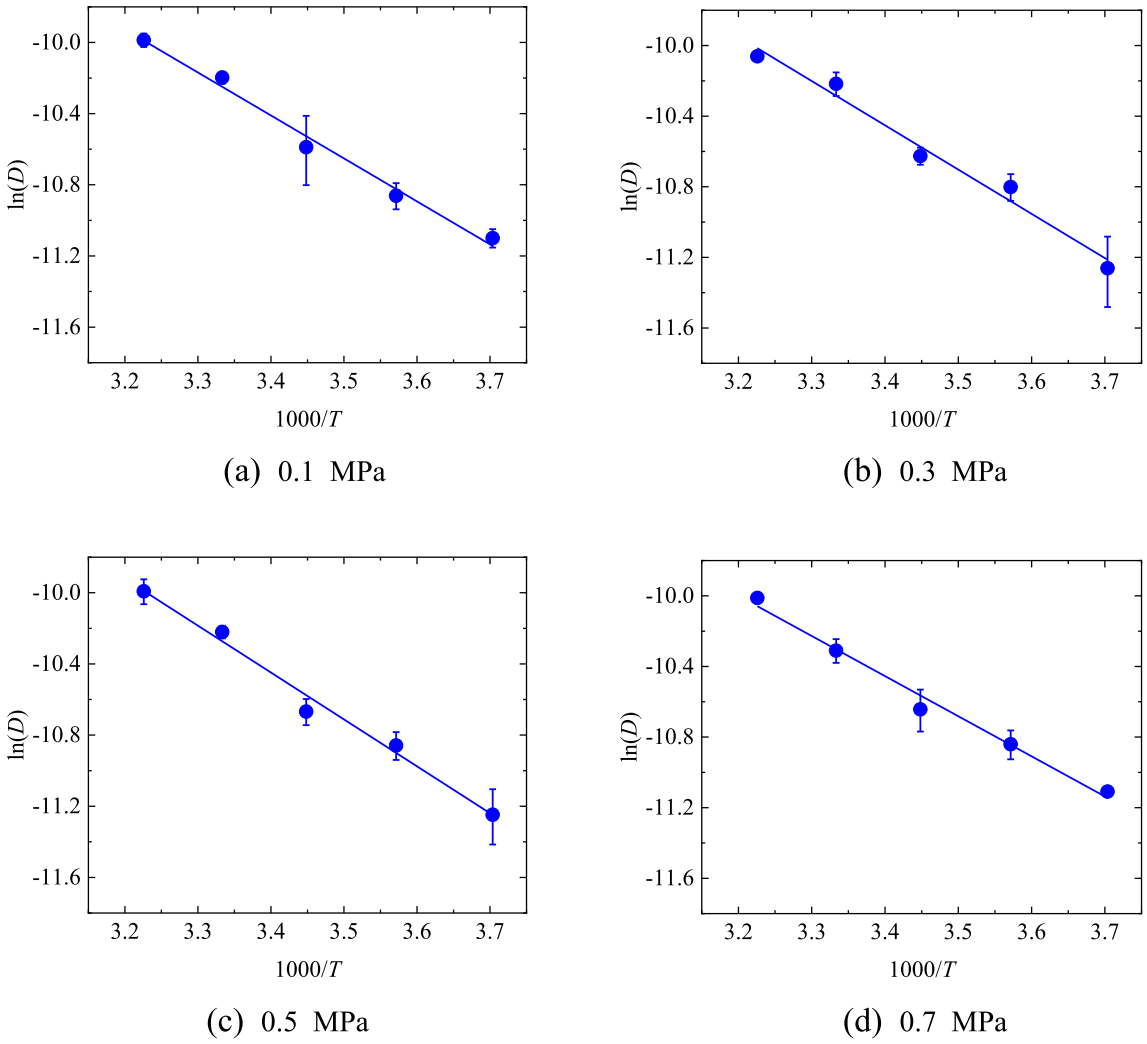

Fig. 11. Relationship between diffusion coefficients and temperatures fitted by the Arrhenius law.

cm^3(STP)/(cm^3·MPa); $\triangle H_s$ is the apparent heat for solution, J/mol; R is the gas constant, J/mol·K; T is the temperature, K.

From Fig. 7, the heat of sorption $\triangle H_s$ in this study is 4346 J/mol, which is very close to the experimental value of 4681 J/mol reported by Deas Jr [45]. However, the $\triangle H_s$ in this study and Deas Jr's [45] are smaller than the value of 9196 J/mol experimentally studied by Ash [42], which can be explained by the experimental results being influenced by different experimental methods and PE materials produced by different processing processes.

5.3. Influences of temperature on the diffusion coefficient

To study the influence of temperature on the diffusion coefficient, the MSD and t are first plotted in logarithmic coordinates, after which the part with a slope of 1 can be found in the log (MSD) – log(t) figure. This denotes normal diffusion, as shown in Fig. 8. The slope a is obtained by linear fitting of the normal diffusion part in the MSD-t figure. According to a, the diffusion coefficient can be obtained using Eq. (13). The relationships between temperatures (270–310 K) and diffusion coefficients at different pressures (0.1–0.7 MPa) are studied, as shown in Fig. 9. It can be clearly observed from Fig. 9 that the diffusion coefficient of H_2 in amorphous PE increases with increasing temperature, which can be attributed to temperature increasing the kinetic energy of H_2, leading to that the H_2 molecules have a great diffusion ability.

The diffusion coefficients of H_2 in amorphous PE with zero crystallinity are studied in this work. Similar to dissolution, the diffusion of H_2 in PE only occurs in the amorphous region of PE but not in the crystalline region; therefore, the degree of crystallinity affects the diffusion coefficient of H_2 in PE. The relationship between the diffusion coefficient of H_2 in amorphous PE and real PE is shown below [47].

$$D_a = \frac{3D_s}{2\theta_a} \tag{17}$$

Here D_a is the diffusion coefficient of gas molecules in amorphous PE materials, cm^2/s; D_s is the diffusion coefficient of gas molecules in semi-crystalline PE materials, cm^2/s; θ_a is the volume fraction of the amorphous region, %.

To validate the results of MD simulation, the diffusion coefficients of H_2 simulated in this study are compared with those of H_2 in the amorphous PE simulated by Zhang [48] through an MD simulation with the COMPASS force field. Additionally, the diffusion coefficients of H_2 in semi-crystalline PE experimentally studied by Ash [42] and Deas Jr [45] are compared, in which the experimental results are transformed into the diffusion coefficient of H_2 in amorphous PE according to Eq. (17). The comparison results are shown in Fig. 10, where the diffusion coefficients predicted by MD simulations are observed to be larger than the experimental diffusion coefficients, which can be attributed to the

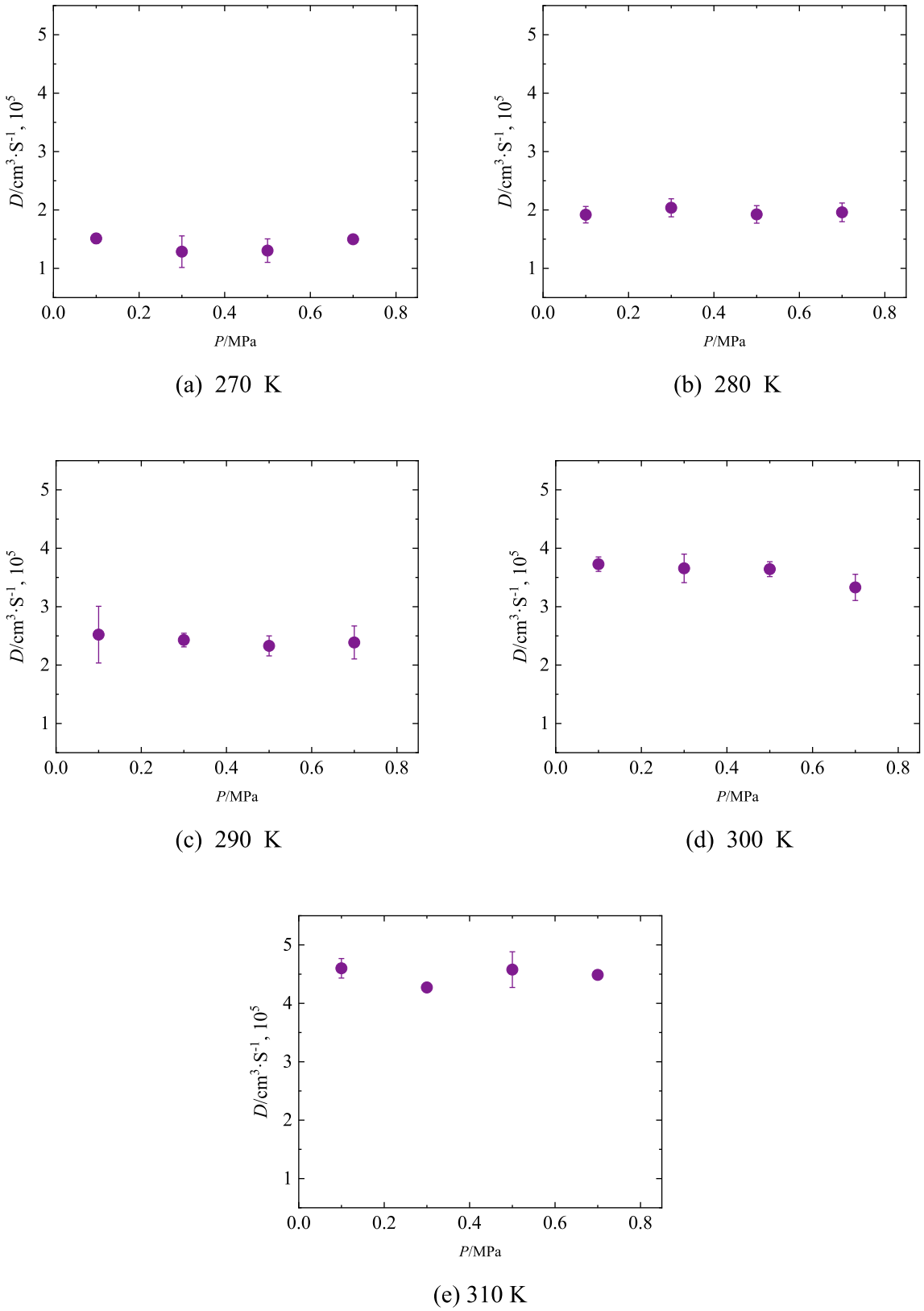

Fig. 12. Diffusion coefficients of H_2 at the pressures of 0.1–0.7 MPa.

following two reasons. First, the simulation results are obtained at the microscopic level, whereas the experimental results are obtained at the macroscopic level. The PE cell used in the MD simulations can not fully reproduce the properties of the real PE materials used in the experiments. Second, Eq. (17) simply transforms the diffusion coefficient of gas in amorphous PE into the diffusion coefficient of gas in semi-crystalline PE. Many factors, such as the length, thickness, and shape of the PE materials, are ignored in

Eq. (17). In general, the simulated diffusion coefficients in this work are of the same order of magnitude and are consistent with the experimental diffusion coefficients, indicating that the MD results in this work with PCFF are reliable.

The relationship between the diffusion coefficients and temperatures of H_2 in amorphous PE can be expressed by the Arrhenius law, as shown in Eq. (18). The fitted results are shown in Fig. 11; here, the logarithm of diffusion coefficients is linear with the reciprocal of temperatures. Thus, when the PE is in the rubbery state, the diffusion coefficients corresponding to other temperatures and at pressures of 0.1–0.7 MPa can be inferred from the Arrhenius law.

$$D = D_0 \times \exp(-\frac{E_d}{RT}) \tag{18}$$

Here D is the diffusion coefficient, cm^2/s; D_0 is the pre-exponential factor corresponding to the diffusion coefficient, cm^2/s; E_d is the apparent activation energy for diffusion, J/mol; R is the gas constant, J/mol·K; T is the temperature, K.

From Fig. 11 (a)–(d), E_d reported in this study are 20078 J/mol, 20852 J/mol, 21907 J/mol and 18898 J/mol, respectively, which are lower than that (32343 J/mol) reported by Deas Jr [45] and close to that (28048 J/mol) determined by Ash [42]. The comparison of the diffusion activation energies illustrates that the results obtained by different experimental methods or instruments will be different. Therefore, it is also normal that there are errors between the MD results and the experimental results. The simulated values are lower than the experimental results, which can be attributed to the fact that the PE cells used in MD are studied at the microscopic level, whereas the real PE materials are investigated at the macroscopic level. Therefore, the difference in scale restricts the agreement between the MD and experimental results.

5.4. Influences of pressure on the diffusion coefficient

To study whether pressure affects the diffusion coefficient of H_2, the relationships between the pressures (0.1–0.7 MPa) and diffusion coefficients at different temperatures (270–310 K) are analyzed. This is shown in Fig. 12; here, it can be observed that the pressure has negligible influence on the diffusion coefficients of H_2 in amorphous PE because the range of simulated pressures is so narrow that the influence of pressure on diffusion is less significant than the error of the calculated results.

5.5. Influences of temperature on the permeability coefficient

By calculating the data in Figs. 5 and 9 using Eq. (14), the permeability coefficients of H_2 in amorphous PE are obtained at the temperatures of 270–310 K and pressures of 0.1–0.7 MPa, as shown in Fig. 13. Here, it can be observed that the permeability coefficient increases with an increase in temperature. Temperature has a significant influence on the permeability coefficients; however, the influence of pressure on the diffusion coefficients shows

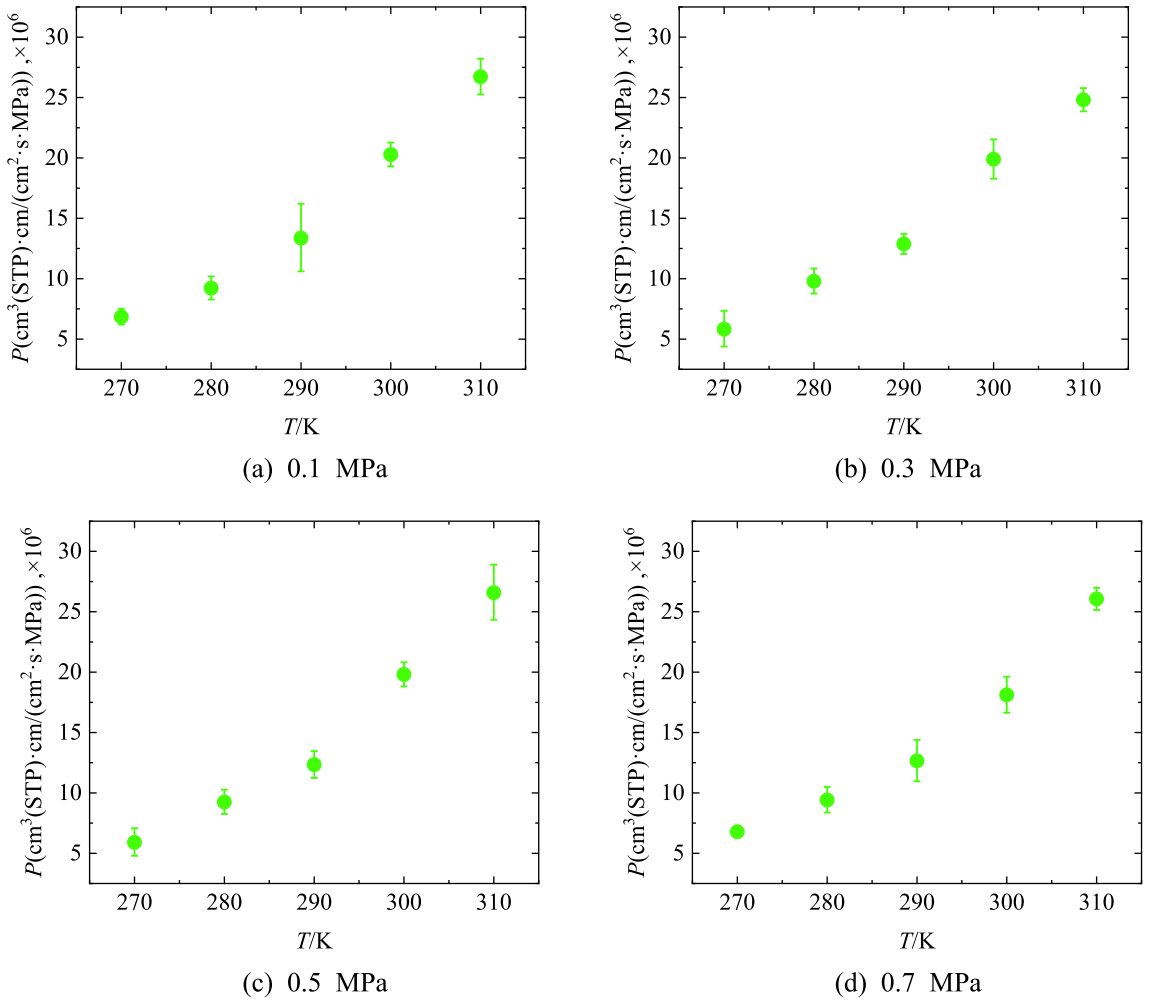

Fig. 13. Permeability coefficients at temperatures of 270–310 K.

that pressure has a negligible effect on the permeability coefficient. In urban gas PE pipelines, the transportation pressure is always low, and the pressure variation range is narrow. Thus, for the permeability performance of H_2, the influence of pressure can be ignored; however, the influence of temperature should be considered. To ensure the safety of the mechanical properties of the pipelines, the urban gas PE pipelines can either be buried much deeper or protected by the insulating layer, to reduce the influence of the surrounding temperature on the PE pipelines. These measures can reduce the permeability of H_2 in urban PE pipelines.

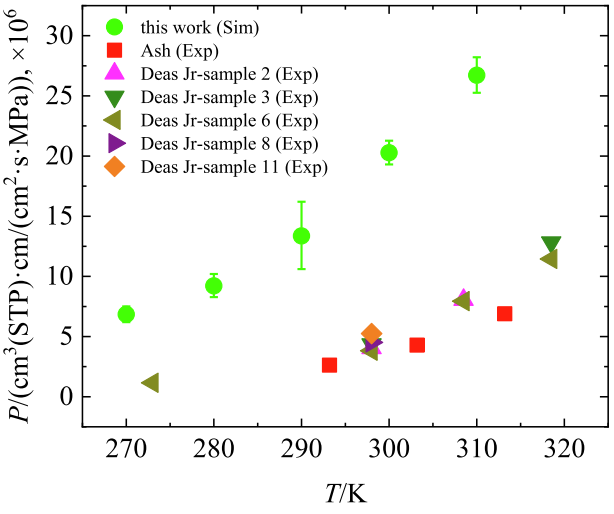

Fig. 14. Comparison of permeability coefficients obtained by MD simulations and experiments at 0.1 MPa.

To facilitate the transformation and calculation of the permeability coefficient of H_2 in amorphous and semi-crystalline PE, Eq. (19) is obtained using Eqs. (14), (15), and (17). The aforementioned relationship can be observed intuitively and easily using Eq. (19).

$$P_a = \frac{3P_s}{2\theta_a^2} \tag{19}$$

Here P_a is the permeability coefficient of gas molecules in amorphous PE materials, $cm^3(STP)\cdot cm/(cm^2\cdot s\cdot MPa)$; P_s is the permeability coefficient of gas molecules in semi-crystalline PE materials, $cm^3(STP)\cdot cm/(cm^2\cdot s\cdot MPa)$; θ_a is the volume fraction of the amorphous region, %.

To validate the simulated permeation results, the permeability coefficients of H_2 obtained in this study are compared with those of H_2 in semi-crystalline PE studied by Ash [42] and Deas Jr [45]. Here, the experimental results are transformed into the permeability coefficient of H_2 in amorphous PE according to Eq. (19), as shown in Fig. 14. In a previous study on the investigation of disso-

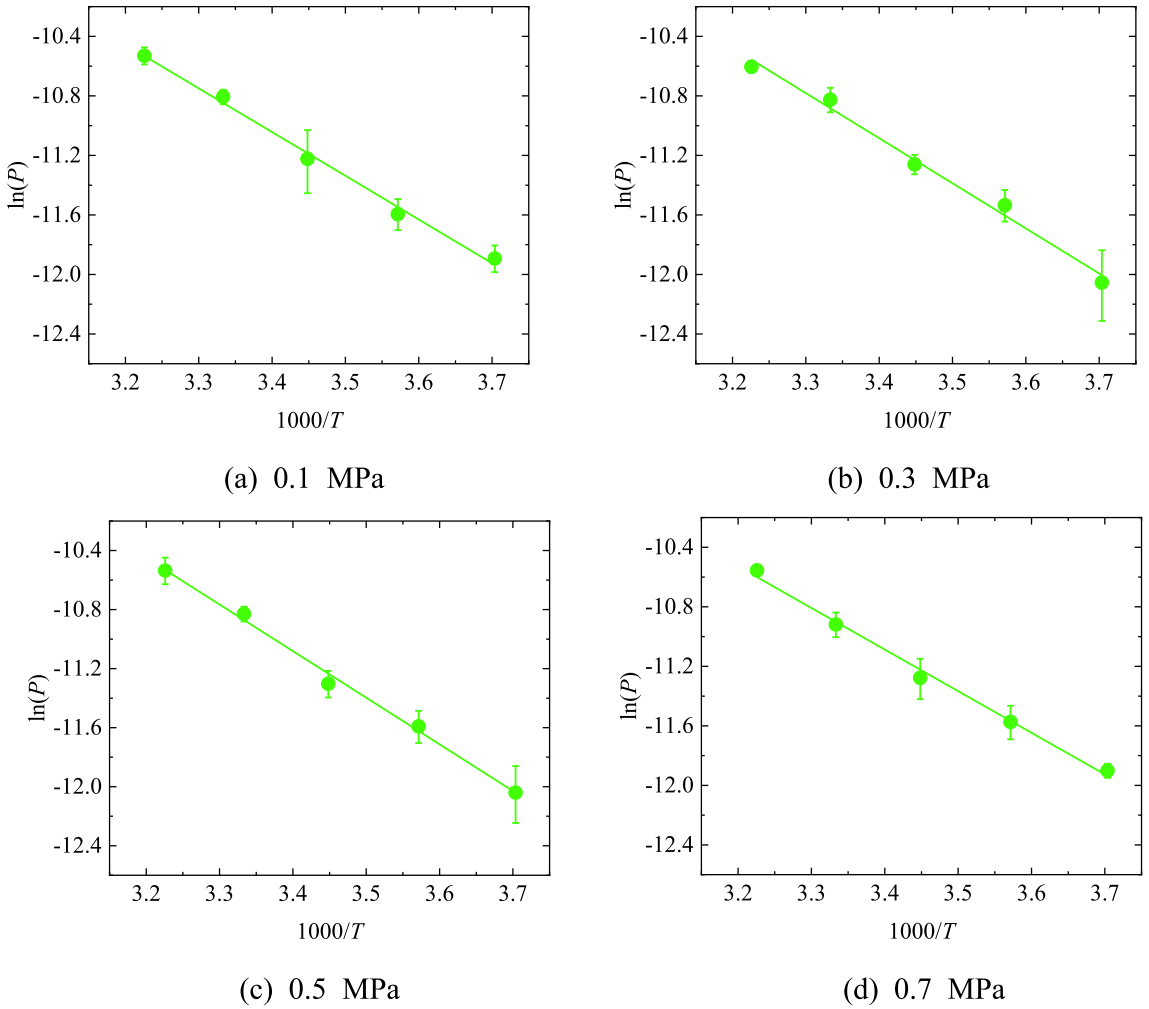

Fig. 15. Relationship between the permeability coefficients and temperatures fitted by the Arrhenius law.

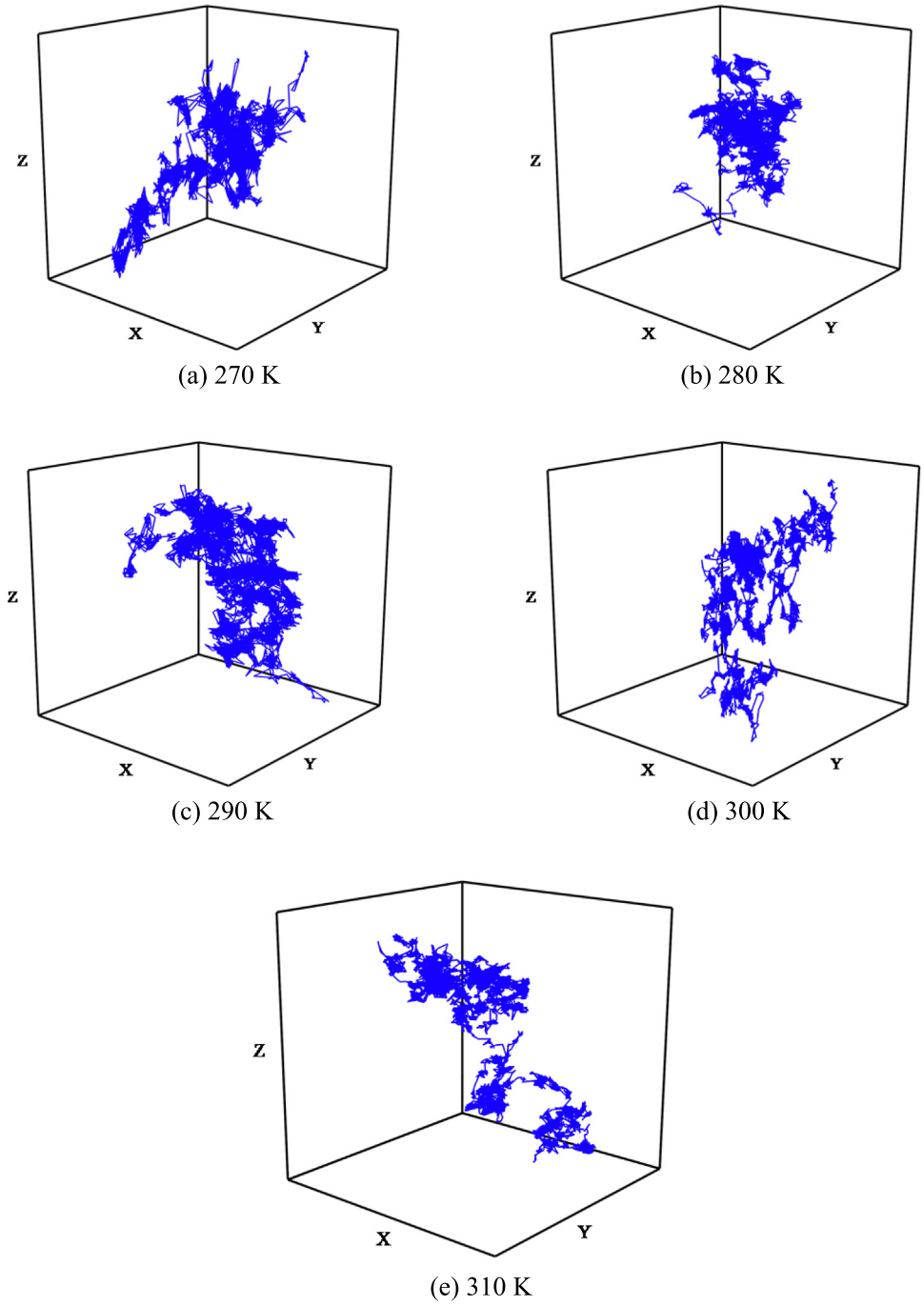

Fig. 16. Comparison of permeability coefficients of H_2 and CH_4 in amorphous PE at 298 K and 0.1 MPa.

lution and diffusion, the solubility and diffusion coefficients obtained by MD are larger than those obtained by Ash [42] and Deas Jr [45]; therefore, the permeability coefficients obtained by MD are also larger than their experimental results according to Eq. (14). The reason for the difference in permeability coefficients is the same as that of the diffusion coefficients, which can be attributed to: (1) the size difference between the PE cell used in MD and real PE used in the experiments; (2) Eq. (19) being a simplified equation that does not consider many other factors.

The relationship between the permeability coefficients and temperatures of H_2 in amorphous PE can also be expressed by the Arrhenius law, as shown in Eq. (20). The fitting results are shown in Fig. 15. Due to the relationship between the solubility coefficient and temperature as well as the diffusion coefficient and temperature conforming to the Arrhenius law, the relationship between the permeability coefficient and temperature should also conform to the Arrhenius law. Similarly, when PE is in the rubbery state, the permeability coefficient under other temperatures at pressures of 0.1–0.7 MPa can be inferred using the Arrhenius law.

$$P = P_0 \times \exp(-\frac{E_p}{RT}) \tag{20}$$

Here P is the permeability coefficient, $cm^3(STP)\cdot cm/cm^2\cdot s\cdot MPa$; P_0 is the pre-exponential factor corresponding to the permeability coefficient, $cm^3(STP)\cdot cm/cm^2\cdot s\cdot MPa$; E_p is the apparent activation

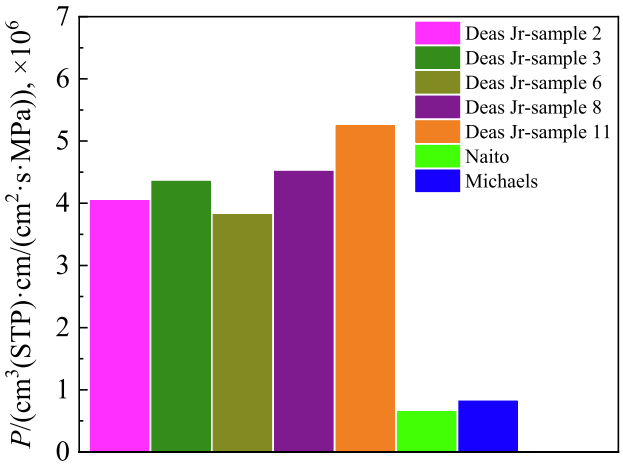

Fig. 17. Diffusion trajectories of H_2 in amorphous PE at different temperatures.

energy for permeation, J/mol; *R* is the gas constant, J/mol·K; *T* is the temperature, K.

In Fig. 15 (a)–(d), E_p simulated in this study are 24427 J/mol, 25200 J/mol, 26256 J/mol and 23238 J/mol, respectively. These simulated values are close to the experimental value of 27000 J/mol and 32172 J/mol reported by Humpenöder [49] and Klopffer [19], but lower than the experimental values of 37026 J/mol and 36342 J/mol obtained by Deas Jr [45] and Ash [42]. Again, it shows that different experiments will get different results, sometimes these results will even differ greatly. The difference between the MD and experimental results can also be attributed to the difference in the scale between the PE cells and real PE materials, which makes the PE cells unable to fully reproduce the properties of the real PE materials.

Urban gas PE pipelines, in which the main component is CH_4, are often used to transport natural gas. However, the gas permeation law changes when H_2 is transported by the PE pipelines because the properties of H_2 are different from those of CH_4. Therefore, the MD results for H_2 and CH_4 in PE are compared and analyzed. At 298 K and 0.1 MPa, the permeability coefficient of CH_4 is 1.40×10^{-7} $cm^3(STP)\cdot cm/cm^2\cdot s\cdot MPa$ in PE with a 57 % amorphous region as studied by Naito, [44] and 0.29×10^{-7} $cm^3(STP)\cdot cm/cm^2\cdot s\cdot MPa$ in PE with a 23 % amorphous region as investigated by Michaels [50]. According to Eq. (20), the permeability coefficients of CH_4 in amorphous PE are obtained and compared with those of H_2 in amorphous PE studied by Deas Jr [45], as shown in Fig. 16. Fig. 16 indicates that the permeability coefficients of H_2 in PE are larger than those of CH_4 in PE. This phenomenon is attributed to the low molecular volume of H_2, which allows the easier permeation of H_2 through PE than CH_4. Therefore, more attention should be paid to the permeation of H_2 when PE pipelines are used to deliver H_2. In addition, the permeability coefficient of H_2 in PE decreases with a decrease in the volume fraction of the amorphous region, according to Eq. (20); therefore, the PE pipeline is recommended to use materials with high crystallinity (low volume fraction of the amorphous region), such as PE100 and PE100-RC, to reduce the permeability of H_2.

5.6. Diffusion mechanism

The diffusion of H_2 in amorphous PE conforms to the "hopping" mechanism. The trajectories and displacements of H_2 in the amorphous PE cell at the temperature of 270–310 K and the pressure of 0.1 MPa are shown in Figs. 17 and 18, respectively. It can be observed that a H_2 molecule vibrates in a certain area for a long time, during which it hops to the adjacent pore in a short time to complete the diffusion. As the H_2 molecule moves away from its initial position over time, the displacement increases as a whole. This phenomenon can be explained in detail as follows: when an H_2 molecule is trapped and vibrates in the pore, the displacement changes slightly, as indicated by the red circle in Fig. 18. Under the action of the thermal motion of PE chains, a channel is generated between two adjacent pores. Subsequently, the H_2 molecule quickly hops to the adjacent pore to complete diffusion through this channel in a short time. A large displacement is produced by the "hopping" process, as shown by the blue circle in Fig. 18. Comparing Fig. 18 (a)–(e), it can be observed that with the increase in temperature, the vibration time decreases and the frequency of the hop increases, which is consistent with the increase in the diffusion coefficient with the increase in temperature.

The diffusion process of the H_2 molecule in amorphous PE is shown in Fig. 19. For convenience, only one H_2 molecule is displayed in the amorphous PE cell, as shown in the yellow color of Fig. 19. The initial position of the H_2 molecule is shown in Fig. 18 (a), and the centroid coordinates of the H_2 molecule are (12.20, 16.65, 45.25). Initially, the H_2 molecule is trapped by the pore and can only vibrate in the pore, as shown in Fig. 19 (b). The centroid coordinates of the H_2 molecule are (11.74, 16.79, 46.36), and the vibration generates a small displacement of 1.21 Å. Under the action of the thermal motion of PE chains, a channel is generated between two adjacent pores, and the H_2 molecule hops to the adjacent pores along the channel because the movement direction of the H_2 molecule is consistent with the channel direction. This is shown in Fig. 19 (c), where the red circle represents the channel and the red arrow represents the hopping direction. At this time, the centroid coordinates of the H_2 molecule are (7.38, 15.79, 45.27), and the displacement generated by hopping is large (4.60 Å). After H_2 molecule hops to a new pore, it continues to vibrate in the new pore and waits for the next hop, as shown in Fig. 19 (d). The centroid coordinates of the H_2 molecule are (8.00, 16.87, 46.04), and the vibration generates a small displacement of 1.46 Å. In Fig. 19, the time step of each process from (a) to (e) is 0.5 ps.

5.7. Free volume

According to the free volume theory of Fox and Flory [51], the volume of the polymer is divided into occupied volume V_o that is occupied by the polymer chain, and free volume V_f that is not occupied by the polymer chain, in which H_2 can only diffuse in the free volume of PE. Increased free volume provides more space for H_2 to diffuse in PE, so that the diffusion coefficient is increased. In this study, the hard probe method is used to investigate the free volume of the amorphous PE cell at different temperatures and pressures. The radius of probe is the van der Waals radius of H_2 (1.4450 Å), which represents the space size of H_2 diffusion in amorphous PE. All H_2 molecules are removed from the amorphous PE cell after the adsorption of H_2 and NPT operation. Finally, amorphous PE cells without H_2 are used as the study objects of the free volume. The effects of temperature and pressure on the free volume of the amorphous PE cell are shown in Figs. 20 and 21, respectively. It can be observed that the free volume increases with an increase in temperature at 0.l MPa, which is consistent with the variation law of the diffusion coefficients and temperatures. The reason for the increase in the diffusion coefficient with increasing temperature is not only the increase in the kinetic energy of H_2, but also the increase in the free volume of PE, which facilitates the diffusion of H_2 molecules in PE. Fig. 21 shows that the free volume changes slightly with an increase in pressure at 270 K, which again indicates that when the variation range of pressure is narrow, the change in pressure has a negligible effect on the diffusion coefficient.

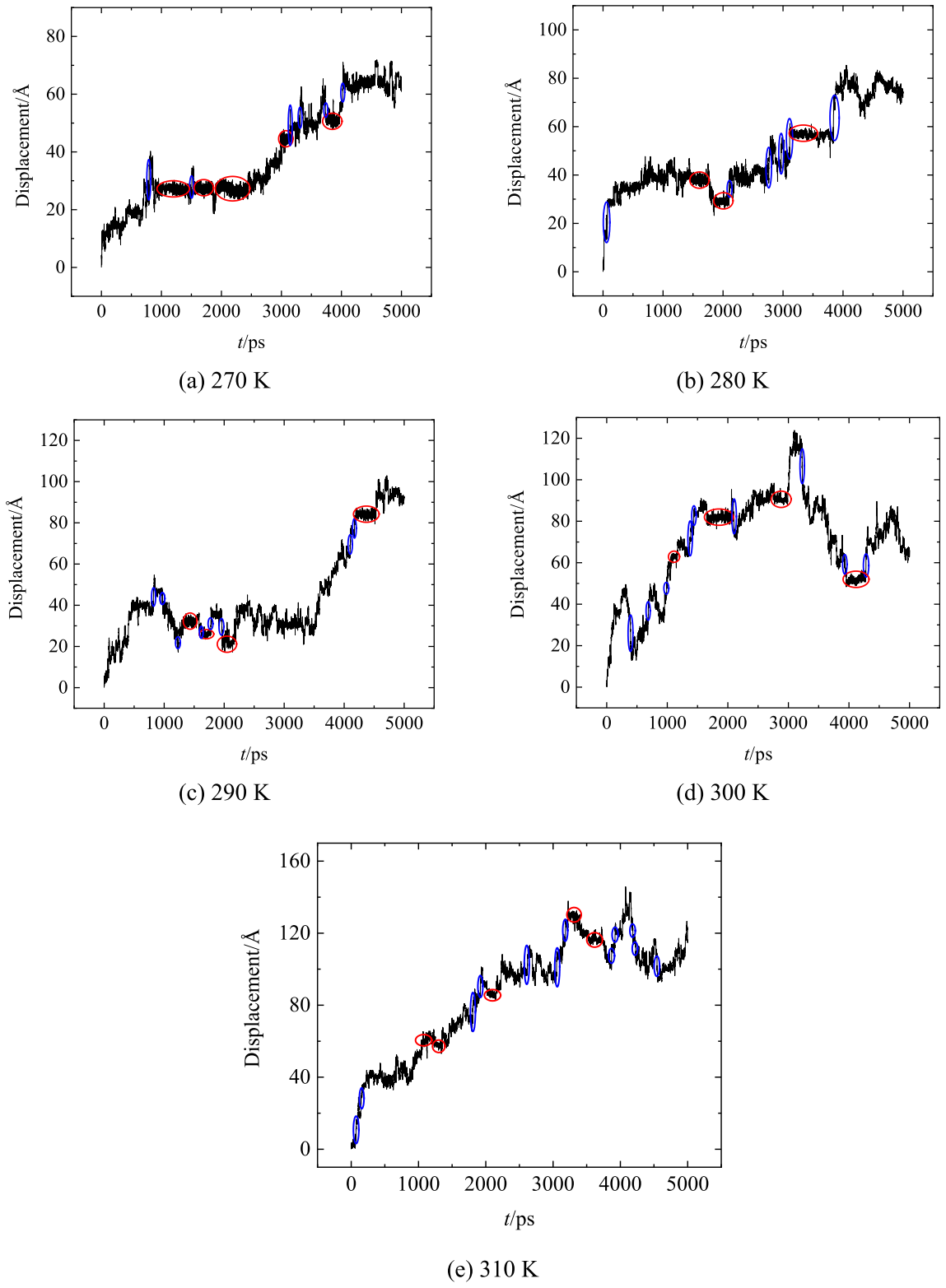

Fig. 18. Displacement of H_2 in amorphous PE at different temperatures.

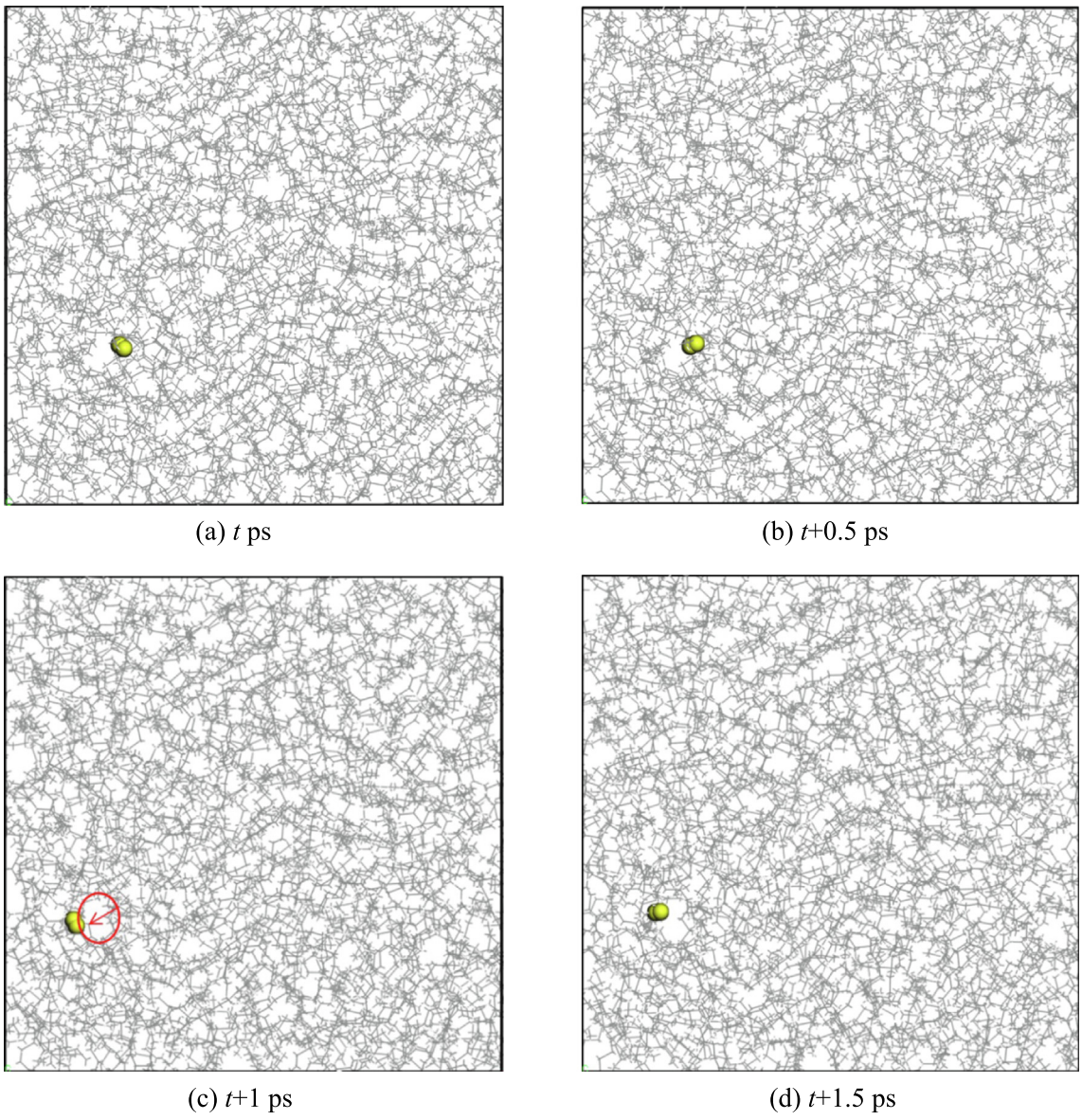

Fig. 19. Diffusion process of H_2 molecule in amorphous PE.

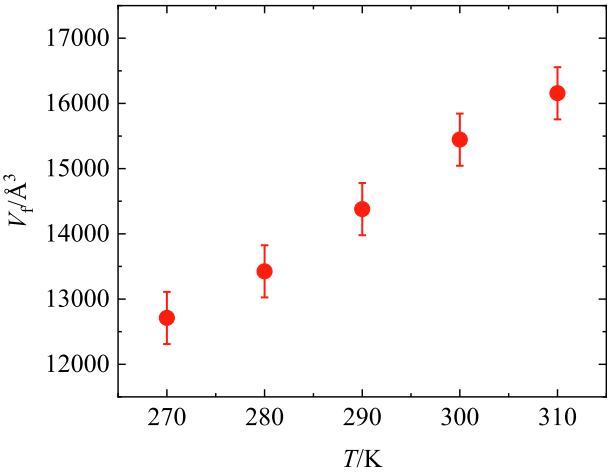

Fig. 20. Free volume of the amorphous PE cell at 0.1 MPa and different temperatures.

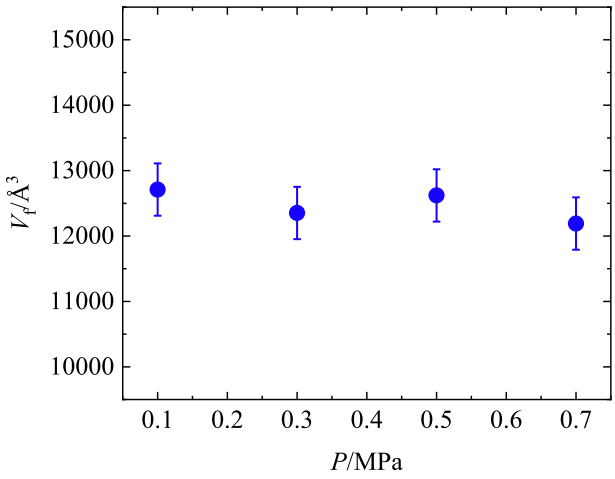

Fig. 21. Free volume of the amorphous PE cell at 270 K and different pressures.

6. Conclusions

Through the GCMC and MD simulations, the solubility, diffusion, and permeability characteristics of H_2 in amorphous PE at temperatures of 270–310 K and pressures of 0.1–0.7 MPa are studied in detail. The following conclusions are drawn.

(1) The solubility, diffusion, and permeability coefficients of H_2 in amorphous PE increase with an increase in temperature. The relationships between the coefficients and temperature conform to the Arrhenius law; thus, the aforementioned coefficients at other temperatures can be inferred from the Arrhenius law.
(2) The influence of pressure on the permeability coefficient is negligible, whereas the influence of temperature on permeability is more significant. Therefore, the deeper burial of urban gas PE pipelines or addition of an insulating layer to reduce the influence of the surrounding temperature can be considered, thereby reducing the permeability of H_2 in PE pipelines. In addition, it is recommended to use PE materials with high crystallinity to transport H_2 to further reduce gas permeability.
(3) The diffusion of H_2 in PE conforms to the "hopping" mechanism. The H_2 molecule vibrates in the pores generated by the free volume for a long time, and the displacement is smaller. Subsequently, the H_2 molecule quickly hops to the adjacent pore in a short time, and the displacement is larger. After the H_2 molecule hops to a new pore, it continues to vibrate and waits for the next hop. The H_2 molecule continuously vibrates and jumps, eventually moving further away from its initial position and permeating through PE.

CRediT authorship contribution statement

Dukui Zheng: Conceptualization, Methodology, Investigation, Validation, Writing – original draft. **Jingfa Li:** Resources, Writing – review & editing, Supervision. **Bing Liu:** Resources, Supervision. **Bo Yu:** Formal analysis, Visualization, Data curation. **Yafan Yang:** Validation, Writing – review & editing. **Dongxu Han:** Methodology. **Jianli Li:** Visualization, Data curation. **Zhiqiang Huang:** Visualization, Supervision.

Data availability

Data will be made available on request.

Declaration of Competing Interest

The authors declare that they have no known competing financial interests or personal relationships that could have appeared to influence the work reported in this paper.

Acknowledgments

This study is supported by the National Key R&D Program of China (2021YFB4001601), the Natural Science Foundation of Jiangsu Province, China (No. BK20221132), and the State Key Laboratory of Engines, Tianjin University (K2022-02).

References

[1] J.F. Li, Y. Su, H. Zhang, B. Yu, Research progresses on pipeline transportation of hydrogen-blended natural gas, Nat. Gas. Ind. 41 (04) (2021) 137–152, https://doi.org/10.3787/j.issn.1000-0976.2021.04.015.
[2] W. Wang, Q.Y. Wang, H.Q. Deng, G.X. Cheng, Y. Li, Feasibility analysis on the transportation of hydrogen–natural gas mixtures in natural gas pipelines, Nat. Gas. Ind. 40 (03) (2020) 130–136, https://doi.org/10.3787/j.issn.1000-0976.2020.03.016.
[3] H. Li, R. Niu, W. Li, H. Lu, J. Cairney, Y.S. Chen, Hydrogen in pipeline steels: Recent advances in characterization and embrittlement mitigation, J. Nat. Gas. Sci. Eng. 105 (2022), https://doi.org/10.1016/j.jngse.2022.104709.
[4] D. Haeseldonckx, W. D'haeseleer, The use of the natural-gas pipeline infrastructure for hydrogen transport in a changing market structure, Int. J. Hydrogen. Energ. 32 (10/11) (2007) 1381-1386, https://doi.org/10.1016/j.ijhydene.2006.10.018.
[5] Y. Gong, S.H. Wang, Z.Y. Zhang, X.L. Yang, Z.G. Yang, H.G. Yang, Degradation of sunlight exposure on the high-density polyethylene(HDPE) pipes for transportation of natural gases, Polym. Degrad. Stabil. 194 (2021), https://doi.org/10.1016/j.polymdegradstab.2021.109752.
[6] B.Q. Sun, L.X. Lu, Y. Zhu, Molecular dynamics simulation on the diffusion of flavor, O_2 and H_2O molecules in LDPE film, Materials. 12 (2019) 3515, https://doi.org/10.3390/ma12213515.
[7] A. Börjesson, E. Erdtman, P. Ahlström, M. Berlin, T. Andersson, K. Bolton, Molecular modelling of oxygen and water permeation in polyethylene, Polymer. 54 (2013) 2988–2998, https://doi.org/10.1016/j.polymer.2013.03.065.
[8] R.C. Dutta, S.K. Bhatis, Transport diffusion of light gases in polyethylene using atomistic simulations, Langmuir. 33 (4) (2017) 936–946, https://doi.org/10.1021/acs.langmuir.6b04037.
[9] Y.F. Yang, A.K.N. Nair, S.Y. Sun, Sorption and diffusion of methane, carbon dioxide, and their mixture in amorphous polyethylene at high pressures and temperatures, Ind. Eng. Chem. Res. 60 (2021) 7729–7738, https://doi.org/10.1021/acs.iecr.0c06110.
[10] A. Hassanzadeh, F. Sabzi, Prediction of CO_2 and H_2 solubility, diffusion, and permeability in MFI zeolite by molecular dynamics simulation, Struct. Chem. 32 (2021) 1641–1650, https://doi.org/10.1007/s11224-021-01743-9.
[11] J.H. Tan, C.L. Chen, Y.W. Liu, J.Y. Wu, D. Wu, X. Zhang, X.Y. He, Z.H. She, R. He, H. L. Zhang, Molecular simulations of gas transport in hydrogenated nitrile butadiene rubber and ethylene–propylene–diene rubber, RSC. Adv. 10 (2020) 12475–12484, https://doi.org/10.1039/d0ra00192a.
[12] A. Brunetti, E. Tocci, M. Cersosimo, J.S. Kim, W.H. Lee, J.G. Seong, Y.M. Lee, E. Drioli, G. Barbieri, Mutual influence of mixed-gas permeation in thermally rearranged poly (benzoxazole-co-imide) polymer membranes, J. Membrane Sci. 580 (2019) 202–213, https://doi.org/10.1016/j.memsci.2019.01.058.
[13] Y. Yi, P. Bi, X.F. Zhao, L.L. Wang, Molecular dynamics simulation of diffusion of hydrogen and its isotopic molecule in polystyrene, J. Polym. Res. 25 (2018) 43, https://doi.org/10.1007/s10965-017-1406-1.
[14] M. Azizi, S.A. Mousavi, CO_2/H_2 separation using a highly permeable polyurethane membrane: molecular dynamics simulation, J. Mol. Struct. 1100 (2015) 401–414, https://doi.org/10.1016/j.molstruc.2015.07.029.
[15] L. Bian, Y. Shu, J. Xu, L. Wang, Molecular dynamics study on permeability of gas molecules through amorphous PPX polymers, Int. Polym. Proc. 28 (1) (2013) 24–33, https://doi.org/10.3139/217.2610.
[16] M.P. Foulc, F. Nony, P. Mazabraud, P. Berne, M.H. Klopffer, B. Flaconneche, G.F. Pimenta, G.M. Syring, I. Alliat, Durability and transport properties of polyethylene pipes for distributing mixtures of hydrogen and natural gas, 16th World Hydrogen Energy Conference (2006), Lyon, France.
[17] M.H. Klopffer, B. Flaconneche, P. Odru, Transport properties of gas mixtures through polyethylene, Plast. Rubber. Compos. 36 (5) (2007) 184–189, https://doi.org/10.1179/174328907X191350.
[18] M.H. Klopffer, P. Berne, S. Castagnet, M. Weber, G. Hochstetter, E. Espuche, Polymer pipes for distributing mixtures of hydrogen and natural gas: Evolution of their transport and mechanical properties after an ageing under an hydrogen environment, 18th World Hydrogen Energy Conference (2010), Essen, Germany.
[19] M.H. Klopffer, B. Flaconneche, Transport properties of polymer pipes for distributing mixtures of hydrogen and natural gas: Development of a new experimental method, Plastics Pipes XIV (2008), Budapest, Hungary.
[20] M.H. Klopffer, P. Berne, É. Espuche, Development of innovating materials for distributing mixtures of hydrogen and natural gas. Study of the barrier properties and durability of polymer pipes, Oil. Gas. Sci. Technol. 70 (2) (2015) 305-315, https://doi.org/10.2516/ogst/2014008.
[21] R.J.M. Hermkens, H. Colmer, H.A. Oohoff. Modern PE pipe enables the transport of hydrogen, Proceedings of the 19th Plastic Pipes Conference (2018), Las Vegas, Nevada.
[22] C. Rizzuto, A. Caravella, A. Brunetti, C.H. Park, Y.M. Lee, E. Drioli, G. Barbieri, E. Tocci, Sorption and diffusion of CO_2/N_2 in gas mixture in thermally-rearranged polymeric membranes: a molecular investigation, J. Membrane Sci. 528 (2017) 135–146, https://doi.org/10.1016/j.memsci.2017.01.025.
[23] J. Sacristan, C. Mijangos, Free volume analysis and transport mechanisms of PVC modified with fluorothiophenol compounds A molecular simulation study, Macromolecules 43 (17) (2010) 7357–7367, https://doi.org/10.1021/ma1011045.
[24] J.H. Tan, C.L. Chen, Y.W. Liu, J.Y. Wu, D. Wu, X. Zhang, Z.H. She, R. He, H.L. Zhang, Molecular simulations of gas transport in hydrogenated nitrile butadiene rubber, J. Polym. Res. 10 (2020) 12475–12484, https://doi.org/10.1007/s10965-020-02258-3.
[25] M. Zhao, C.L. Zhang, F. Yang, Y.X. Weng, Gas barrier properties of furan-based polyester films analyzed experimentally and by molecular simulations, Polymer. 233 (2021), https://doi.org/10.1016/j.polymer.2021.124200.
[26] H.L. Liu, X.J. Ding, J. Yi, L.Q. Zhang, S.Z. Wu, Study on the gas permeabilities in styrene-butadiene rubber by molecular dynamics simulation, Front. Chem. Sci. Eng. 4 (3) (2010) 257–262, https://doi.org/10.1007/s11705-009-0270-x.

[27] D.N. Theodorou, U.W. Suter, Detailed molecular structure of a vinyl polymer glass, Macromolecules. 18 (1985) 1467–1478, https://doi.org/10.1021/ma00149a018.
[28] D.N. Theodorou, U.W. Suter, Atomistic modeling of mechanical properties of polymeric glasses, Macromolecules. 19 (1986) 139–154, https://doi.org/10.1021/ma00155a022.
[29] H.B. Li, X.M. Zhang, H.F. Chu, G.Q. Qi, H. Ding, X. Gao, J.X. Meng, Molecular simulation on permeation behavior of $CH_4/CO_2/H_2S$ mixture gas in PVDF at service conditions, Polymers. 14 (3) (2022) 545, https://doi.org/10.3390/polym14030545.
[30] J.K. Adewole, L. Jensen, U.A. Al-mubaiyedh, N.V. solms, I.A. Hussein, Transport properties of natural gas through polyethylene nanocomposites at high temperature and pressure, J. Polym. Res. 19 (2) (2012) 9814, https://doi.org/10.1007/s10965-011-9814-0.
[31] G.J. Gao, H. Zhao, W.F. Sun, Molecular dynamics simulation study of parallel orientation structure and gas transport in graphite-nanoplatelet/polyethylene composites, Mater. Today. Commun. 13 (2017) 57–64, https://doi.org/10.1016/j.mtcomm.2017.08.004.
[32] C. Peng, F.L. Zeng, A molecular simulation study to the deformation Behaviors and the size effect of polyethylene during nanoindentation, Comp. Mater. Sci. 137 (2017) 225–232, https://doi.org/10.1016/j.commatsci.2017.05.044.
[33] K. Golzar, S. Amjad-iranagh, M. Amani, H. Modarress, Molecular simulation study of penetrant gas transport properties into the pure and nanosized silica particles filled polysulfone membranes, J. Membrane. Sci. 451 (2014) 117–134, https://doi.org/10.1016/j.memsci.2013.09.056.
[34] R.A. Luke, Q. Yang, M.E. Andrew, Comparing gas transport in three polymers via molecular dynamics simulation, Phys. Chem. Chem. Phys. 20 (2018) 22123–22133, https://doi.org/10.1039/C8CP02829J.
[35] D.J. Branken, H.M. Krieg, G. Lachmann, P.A.B. Carstens, Modelling sorption and diffusion of NF_3 and CF_4 in Teflon AF perfluoropolymer membranes, J. Membrane. Sci. 470 (2014) 294–306, https://doi.org/10.1016/j.memsci.2014.07.033.
[36] C.H. Lu, S.J. Ni, W.K. Chen, L.S. Liao, C.J. Zhang, A molecular modeling study on small molecule gas transportation in poly (chloro-p-xylylene), Comp. Mater. Sci. 49 (2010) S65–S69, https://doi.org/10.1016/j.commatsci.2010.01.044.
[37] M.H. Klopffer, B. Flaconneche, Transport properties of gases in polymers: Bibliographic review, Oil. Gas. Sci. Technol. 56 (3) (2001) 223–244, https://doi.org/10.2516/ogst:2001021.
[38] H.F. Lu, Z.P. Zhou, T.F. Hao, X.B. Ye, Y.J. Ne, Temperature dependence of structural properties and chain configurational study: a molecular dynamics simulation of polyethylene chains, Macromol. Theor. Simul. 24 (2015) 335–343, https://doi.org/10.1002/mats.201500007.
[39] Y. Sato, M. Yurugi, K. Fujiwara, S. Takishima, H. Masuoka, Solubilities of carbon dioxide and nitrogen in polystyrene under high temperature and pressure, Fluid. Phase. Equilibr. 125 (1–2) (1996) 129–138, https://doi.org/10.1016/s0378-3812(96)03094-4.
[40] Y. Sato, K. Fujiwara, T. Takikawa, S. Sumarno, H.M. Takishima, Solubilities and diffusion coefficients of carbon dioxide and nitrogen in polypropylene, high-density polyethylene, and polystyrene under high pressures and temperatures, Fluid Phase. Equilibr. 162 (1–2) (1999) 261–276, https://doi.org/10.1016/S0378-3812(99)00217-4.
[41] A.S. Michaels, H.J. Bixler, Solubility of gases in polyethylene, J. Polym. Sci. 50 (154) (1961) 393–412, https://doi.org/10.1002/pol.1961.1205015411.
[42] R. Ash, R.M. Barrer, D.G. Palmer, Solubility and transport of gases in nylon and polyethylene, Polymer. 11 (8) (1970) 421–435, https://doi.org/10.1016/0032-3861(70)90004-2.
[43] M.J. Chen, Investigation of the sorption and diffusion in polyethylene by gravimetric and NMR methods and its application, Hangzhou: Zhejiang University (2014), PhD dissertation.
[44] Y. Naito, K. Mizoguchi, K. Terada, Y. Kamiya, The effect of pressure on gas permeation through semicrystalline polymers above the glass transition temperature, J. Polym. Sci. Pol. Phys. 29 (4) (1991) 457–462, https://doi.org/10.1002/polb.1991.090290408.
[45] T.M. Deas Jr, H.H. Hofer, M. Dole, Solubility of hydrogen in polyethylene by a semimicro method, Macromolecules. 5 (2) (1972) 223–226, https://doi.org/10.1021/ma60026a023.
[46] S. Kubo, M. Dole, A method for the determination of the solubility of hydrogen in polyethylene, Macromolecules. 6 (5) (1973) 774–777, https://doi.org/10.1021/ma60035a025.
[47] P.V.K. Pant, R.H. Boyd, Molecular-dynamics simulation of diffusion of small penetrants in polymers, Macromolecules. 26 (4) (1993) 679–686, https://doi.org/10.1021/ma00056a019.
[48] L.S. Zhang, Y.G. Wang, G. Wu, S.Z. Wu, L.Q. Zhang, Study on the gas diffusion in olefin copolymer membrane by molecular dynamics simulation, Sci. Tech. Rev. 26 (12) (2008) 52–57, https://doi.org/10.3321/j.issn:1000-7857.2008.12.010.
[49] J. Humpenöder, Gas permeation of fibre reinforced plastics, Cryogenics. 38 (1) (1998) 143–147, https://doi.org/10.1016/S0011-2275(97)00125-2.
[50] A.S. Michaels, H.J. Bixler, Flow of gases through polyethylene, J. Polym. Sci. 50 (154) (1961) 413–439, https://doi.org/10.1002/pol.1961.1205015412.
[51] T.G. Fox, P.J. Flory, Second-order transition temperatures and related properties of polystyrene. I. Influence of molecular weight, J. Appl. Phys. 21 (6) (1950) 581–591, https://doi.org/10.1063/1.1699711.